

Modeling Structural Coordination and Ligand Binding in Zinc Proteins with a Polarizable Potential

Jiajing Zhang,[†] Wei Yang,^{‡,§} Jean-Philip Piquemal,^{||,⊥} and Pengyu Ren^{*,†}

[†]Department of Biomedical Engineering, The University of Texas at Austin, Texas 78712, United States

[‡]The Institute of Molecular Biophysics and [§]Department of Chemistry and Biochemistry, Florida State University, Tallahassee, Florida 32306, United States

^{||}UPMC Univ. Paris 06, UMR 7616, Laboratoire de Chimie Théorique, case courrier 137, 4 place Jussieu, F-75005, Paris, France

[⊥]CNRS, UMR 7616, Laboratoire de Chimie Théorique, case courrier 137, 4 place Jussieu, F-75005, Paris, France

S Supporting Information

ABSTRACT: As the second most abundant cation in the human body, zinc is vital for the structures and functions of many proteins. Zinc-containing matrix metalloproteinases (MMPs) have been widely investigated as potential drug targets in a range of diseases ranging from cardiovascular disorders to cancers. However, it remains a challenge in theoretical studies to treat zinc in proteins with classical mechanics. In this study, we examined Zn^{2+} coordination with organic compounds and protein side chains using a polarizable atomic multipole-based electrostatic model. We find that the polarization effect plays a determining role in Zn^{2+} coordination geometry in both matrix metalloproteinase (MMP) complexes and zinc-finger proteins. In addition, the relative binding free energies of selected inhibitors binding with MMP13 have been estimated and compared with experimental results. While not directly interacting with the small molecule inhibitors, the permanent and polarizing field of Zn^{2+} exerts a strong influence on the relative affinities of the ligands. The simulation results also reveal that the polarization effect on binding is ligand-dependent and thus difficult to incorporate into fixed-charge models implicitly.

■ INTRODUCTION

One third of all proteins contain metal ions as their integral parts.¹ The metal ions in these protein complexes serve essential biological functions, from organizing the secondary or tertiary structure, facilitating protein–ligand interactions, to directly participating in catalytic activities. Many metalloproteins, similar to the ion channels, recognize and associate with only specific types of ions against a solution of various ions of similar properties (e.g., charge and size). For example, calmodulin, involved in signal transduction, DNA synthesis, and cell division, undergoes significant conformational changes upon binding to Ca^{2+} ;² protein kinases and ATPase require Mg^{2+} in coordination with ATP to facilitate phosphoryl transfer.^{3,4} Metalloenzymes, such as alcohol dehydrogenase, carboxypeptidase, thermolysin, and matrix metalloproteinases (MMPs), rely on Zn^{2+} for their catalytic activities.⁵ As the second most abundant cation in the human body,⁶ Zn has important biological implications and is involved in the survival and pathogenesis of many viruses, including HIV, hepatitis, herpes simplex, Rubella, and influenza.^{7–11}

In aqueous solution, it is well established that Zn^{2+} has a coordination number of six and forms an octahedral structure with water. When binding in the protein complexes, a tetrahedral arrangement with the surrounding amino acid residues is often observed, although Zn^{2+} can also exist in a five- or a six-coordinated complex. In protein, Zn^{2+} can serve either a catalytic role, by participating directly in chemical catalysis, or a structural role solely to maintain protein structure and stability.¹² Analysis of protein X-ray structures shows that, among 126 structural proteins, a majority of the zinc sites

(82%) are 4-coordinated, only 14% are 5-coordinated, and 4% are 6-coordinated. Of 147 catalytic binding proteins, 58% are 4-coordinated, 31% are 5-coordinated, and 11% are 6-coordinated.¹³ Therefore, tetrahedral coordination is dominant in proteins, although a significant amount of zinc ions display higher coordination numbers. Common ligands for the zinc ion include histidine, aspartate or glutamate, and cysteine, in a variety of combinations. The flexibility in the ligand choices and coordination geometries leads to diverse Zn^{2+} binding sites in zinc metalloenzymes, rendering possible a range of important biological roles, such as catalytic, coactive, and structural functions.¹⁴

A computational study of zinc ions embedded in a protein active site has been a long-standing challenge. While Quantum Mechanics¹⁵ or combined Quantum Mechanics/Molecular Mechanics methods^{16,17} have been applied to investigate zinc-containing molecular systems, the computational cost of high level *ab initio* calculations makes it difficult to tackle complex configurational space or long-time dynamics. On the other hand, classical mechanics treatment of Zn^{2+} is problematic. The strong local electrostatic field and induction effect¹⁸ pose challenges for the traditional fixed-charge molecular mechanics^{19–21} and quantum chemistry methods^{22,23} to model zinc ions in biomolecules.

Two types of approaches have been implemented in a fixed-charge force field: nonbonded and bonded models. The nonbonded model presented by Stote and Karplus²⁴ is widely

Received: November 11, 2011

Published: February 13, 2012

used due to its simplicity and efficiency in the investigation of the structure, dynamics, and energetics of zinc-containing proteins. For example, Donini and Kollman reported studies on inhibitors binding to matrix metalloproteinases based on such a nonbonded description for Zn^{2+} .²⁰ However, it is generally believed that treating zinc metal in a nonbonded fashion leads to an overly strong preference for octahedral coordination, and sometimes the zinc ion even escapes from the coordination sphere. It has also been reported that the nonbonded model is not able to properly describe the coordination number and energy at the same time.²⁵ Many have attempted to use artificial bonds between ion and ligand atoms to fix the geometry for the purposes of modeling ion–ligand interactions, which is referred to as the bonded model.^{26–28} A semibonded model with tetrahedral charge dummies around zinc has also been proposed.²⁹ By placing four cationic dummy atoms tetrahedrally around the zinc nucleus, the orientation requirement for the zinc coordinates is imposed all the time during the simulation. The extra charge sites however give rise to unphysical permanent dipole and quadrupole moments to the Zn^{2+} . These bonded or semibonded models and their variant methods freeze the specific zinc coordination to the surroundings, which will likely cause artifacts on the ligand conformational sampling and dynamics. The inability to model zinc has been a hindrance to understanding the versatile functions of Zn^{2+} and metalloenzymes, given that the variability in Zn^{2+} coordination may be coupled with enzyme function at different stages of the reaction.⁶ The lack of charge transfer and explicit polarizability can result in poor accuracy for the association energies.³⁰ Classical nonpolarizable force fields are inherently unsuitable for describing flexible zinc coordination.

Polarizable potentials hold promise as they explicitly account for polarization and even charge-transfer effects. SIBFA was one of the first potentials developed to model Zn interaction with organic and biological molecules by rigorously incorporating polarization, charge transfer, penetration, and other effects.^{31–37} Gresh reported the very first attempt to introduce an explicit charge transfer energy term in Zn^{2+} modeling and this work systematically monitored the distal and angular dependencies against quantum chemistry energy decomposition in various Zn^{2+} ligand complexes.³³ A critical feature of charge transfer effect relates to its nonadditive behavior in polyligated complexes, which was monitored against quantum chemistry computations by Tiraboschi et al.^{36,37} The penetration effect was also introduced for Zn by Gresh and co-workers in their subsequent work.³² The applications of SIBFA to model the complexes of inhibitors to a Zn-metalloenzyme, thermolysin, were initiated early in 1997–1998,^{34,35} followed by applications to β -lactamase,^{38,39} Zn-fingers,⁴⁰ and phosphomannoisomerase.^{41,42} Sakharov and Lim also developed a model which reproduced the experimentally observed tetrahedral structures of Cys_2His_2 and Cys_4 Zn-binding sites in proteins.⁴³ The treatment by Sakharov and Lim simply introduced distance-dependent partial charges on zinc without actually accounting for the second order charge-transfer effect. It is interesting to note that reduced partial charges lead to less favorable Coulombic interactions, opposite of what one expects from a charge-transfer effect.

Previously, we developed a polarizable multipole-based model for Zn^{2+} in a water environment.¹⁸ In this study, we are extending the polarizable model to investigate zinc binding with organic molecules and proteins. Three molecules, the acetate anion, the methanethiol anion (CH_3S^-), and imidazole,

were selected to mimic the side chains of typical Zn^{2+} -interacting ligands, Asp, Cys, and His. Two zinc enzyme systems with different coordination ligands (Asp, His, Cys, water) have been examined using MD simulations (Figure 2): system A is a zinc-finger with three 4-fold coordinated zinc structural sites, and system B is a matrix metalloproteinase (MMP) complex with two 4-fold coordinated zinc sites, one catalytic and the other structural zinc.

The Cys_2His_2 -type zinc-finger protein consists of highly conserved zinc finger domains where each zinc ion is coordinated by two cysteines and two histidines. Each domain consists of two β strands, one α helix, and a hairpin structure. Three residues located at the α helices in each finger interact with three nucleotide bases of the DNA, typically making contacts with contiguous three base pair recognition sites. Such a direct recognition mode to DNA makes zinc finger proteins an ideal scaffold for designing proteins that can recognize the predetermined DNA sequences specifically.⁴⁴ During the zinc-finger protein folding process, zinc ions play a crucial role by binding to the peptides first, then directing the folding and stabilizing the β -hairpin and α -helix as suggested by Li et al.⁴⁵

The other Zn-containing protein investigated here is MMP, which belongs to a family of zinc-dependent endopeptidases related to the physiological homeostasis of the extracellular matrix. Abnormal expression of MMPs has been implicated in a number of pathological conditions such as metastasis, angiogenesis, osteoarthritis, rheumatoid arthritis, and cardiovascular diseases. The development of selective and potent inhibitors to MMPs is a topic of considerable interest.^{46–50} A number of computational studies of inhibitors binding to MMPs have been reported.^{19,20,48,51} A majority of available MMP inhibitors are zinc chelating compounds containing zinc binding groups (ZBG), such as hydroxamate (CONH-O^-), carboxylate (COO^-), thiolate (S^-), or phosphinate (PO_2^-).⁵² Unfortunately, these inhibitors are often found to be biologically labile, lacking selectivity, or having toxic side effects.⁵³ Considerable efforts have also been made to develop nonzinc chelating compounds that lead to inhibitors with specificity to certain MMP subtypes.^{54,55}

■ COMPUTATIONAL METHODS

The Polarizable Force Field and Parametrization. In the AMOEBA force field, permanent atomic multipoles up to quadrupoles are used to describe electrostatic interactions. The polarization effect is explicitly accounted for by incorporating dipole induction in a self-consistent manner.⁵⁶ A buffered 14–7 potential is used to describe the repulsion–dispersion interactions between pairs of nonbonded atoms.⁵⁷ Parameters for all proteins and existing small molecules involved in this study were taken from the AMOEBA force field.⁵⁸ Previously, the AMOEBA polarizable multipole based force field has been applied to study water,^{59,60} monovalent and divalent ions,^{18,61–63} organic molecules and peptides,^{56,64,65} protein–ligand binding prediction,^{66,67} and computational X-ray crystallography^{68–70} with very encouraging success. A number of independent studies on ions^{71–76} and peptides using AMOEBA also demonstrated the improvements and advantages offered by the polarizable force field.^{77–80}

Zn^{2+} electrostatic parameters include a point charge (+2) and an atomic polarizability.¹⁸ In the AMOEBA force field, Thole damping is achieved by the screening of pairwise atomic multipole interactions and is equivalent to replacing a point

multipole moment with a smear charge distribution. The damping function for charges is given by functional form⁸¹

$$\rho = \frac{3a}{4\pi} \exp(-au^3) \quad (1)$$

where $u = r_{ij}/(\alpha_i\alpha_j)^{1/6}$ is the effective distance as a function of linear separation r_{ij} and the atomic polarizabilities of sites i (α_i) and j (α_j). The coefficient a is the dimensionless width of the smeared charge distribution and controls the damping strength. The corresponding damping functions for charge, dipole, and quadrupole interactions were reported previously.⁵⁹ A single transferable isotropic polarizability for each common chemical element was derived by fitting to experimental polarizabilities of a set of representative organic molecules. Except for the aromatic atoms and atoms with formal charges (details below), the atomic polarizabilities as originally suggested by Thole were adopted in the AMOEBA force field, i.e., 1.334 Å³ for carbon, 0.496 Å³ for hydrogen, 1.073 Å³ for nitrogen, and 0.837 Å³ for oxygen (Table 2). The parameters for Zn and water were published previously¹⁸ and are used in this study.

The *ab initio* calculation of the molecular polarizability tensor of three model compounds was performed at the level of MP2/6-311++G(2d,2p) (see Table 1). These molecular polarizability

Table 1. Comparison of Molecular Polarizabilities (Å³) from *ab Initio* Quantum Mechanical, AMOEBA Polarizable Model Prediction, and Experimental Measurement

		<i>ab initio</i> ^a	AMOEBA	other exptl or calcd
CH ₃ COO ⁻	α_{xx}	7.12	6.09	7.34 ^b
	α_{yy}	6.95	5.71	7.49 ^b
	α_{zz}	4.58	4.47	4.91 ^b
	α_{total}	6.21	5.42	6.58 ^b
CH ₃ S ⁻	α_{xx}	6.97	5.34	
	α_{yy}	6.97	5.34	
	α_{zz}	8.42	7.14	
	α_{total}	7.45	5.94	4.3; ^c 4.4; ^c 5.5; ^c 6.7 ^c
C ₃ N ₂ H ₄ (imidazole)	α_{xx}	8.09	9.44	9.6 ^d
	α_{yy}	7.97	8.81	8.6 ^d
	α_{zz}	4.88	5.39	6.6 ^d
	α_{total}	6.98	7.88	8.24; ^d 7.5 ^e

^aCalculated at the level of MP2/6-311++G(2d,2p). ^bCalculation from ref 104. ^cCalculation from ref 105. ^dExperimental measurement from ref 106. ^eRef 107.

tensor values were used to verify and refine the atomic polarizability of aromatic atoms (C, N, and H) and atoms with formal charges (O⁻ and S⁻). The final values of standard and adjusted atomic polarizabilities are compared in Table 2.

Permanent atomic multipole parameters of the charged model compounds, the acetate anion (COO⁻), the methanethiol anion (CH₃S⁻), and imidazole, were derived in this study from *ab initio* QM calculations. Specifically, the permanent multipole moments were derived using the original Distributed Multipole Analysis (DMA) method from the density matrix output at the level of MP2/6-311G** using the GDMA software⁸² and then optimized to reproduce the *ab initio* QM electrostatic potential from a higher level basis set (e.g., MP2/aug-cc-pVTZ) using TINKER.⁸³

Finally, the Zn²⁺-model compound dimer and water-model compound dimer (Figure 1) interaction energy profiles were evaluated by both the AMOEBA and *ab initio* methods (at the

Table 2. AMOEBA Force Field Parameters Derived from *Ab Initio* Zn²⁺ Model Compound Structure and Interaction Energy

	polarizability(Å ³)	vdW r/ϵ
O	0.837	1.650/0.1120
O ⁻	1.600	1.850/0.1290
S	2.800	2.0025/0.3550
S ⁻	4.000	2.100/0.3550
N	1.073	
N (aromatic)	1.500	
C	1.334	
C (aromatic and COO ⁻)	1.750	
H	0.496	
H (aromatic)	0.696	

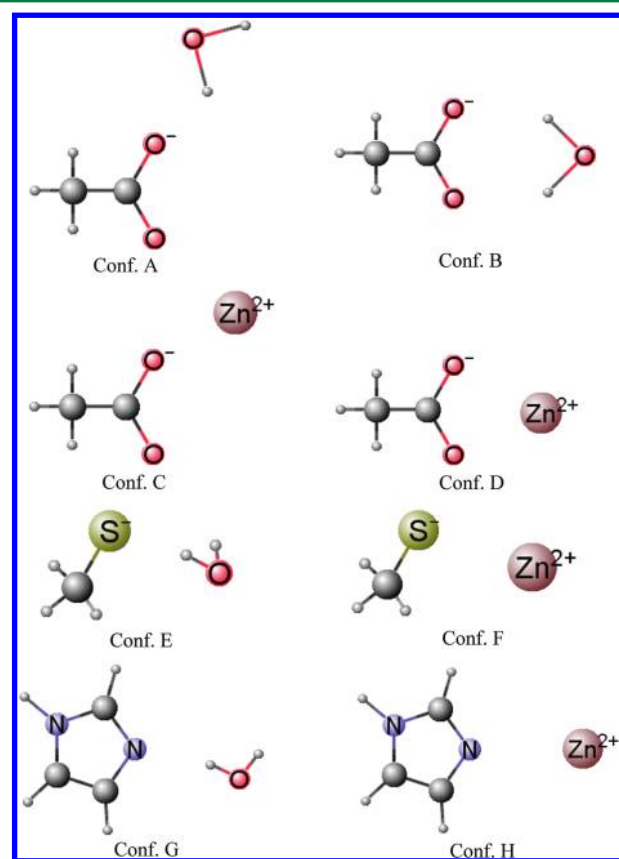


Figure 1. The model systems studied with QM and AMOEBA.

level of MP2/Aug-cc-pvtz with BSSE corrections) using TINKER⁸³ and Gaussian 03,⁸⁴ respectively (see the Supporting Information). Both the *ab initio* and AMOEBA results were compared at the same geometries, which were minima on the QM surface for different radial variations. The dimer energy was evaluated as the difference between the dimer and monomer energy values, without relaxing the monomer geometry. The missing vdW AMOEBA parameters of the ionic model compounds were fitted to reproduce the *ab initio* dimer energy, with the electrostatic parameters fixed. The resulting parameters from the model compounds are then transferred to the side chains of the residues for the Zn protein MD simulations (Table 2).

For the four pyrimidine dicarboxamide inhibitors in MMP complexes (Figure 6), the equilibrium bond and angle values were obtained from the QM (at the level of HF/6-31G*)

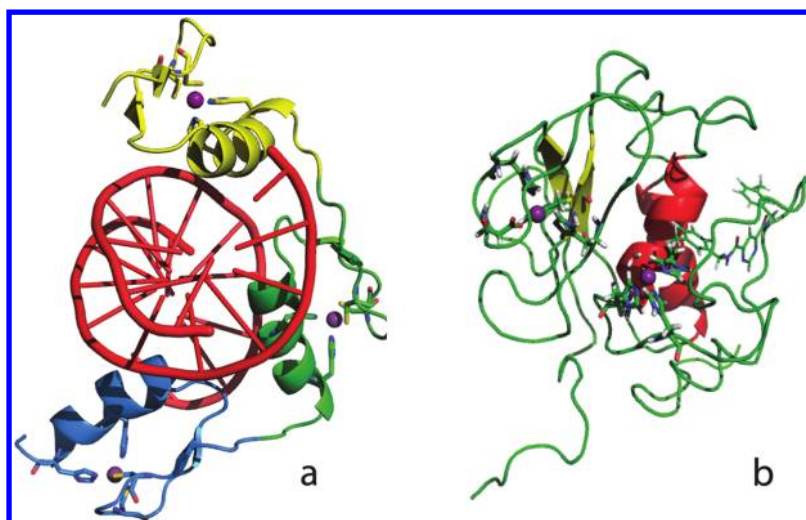


Figure 2. Crystal structures of Zinc-finger protein in complex with DNA (PDB entry: 1AAY, panel a) and MMP13 protein (PDB entry: 1XUD, panel b). In panel a, the DNA is shown in red cartoon representation; the three zinc finger motifs are illustrated in yellow, green, and blue, respectively. In panel b, the α helices are in red, beta sheets are in yellow, and the ligand is in line representation. In both panels, the zinc ions are in purple, and zinc-coordinating residues are in stick representation.

optimized geometry of the ligands. The same procedure described above is used to acquire permanent atomic multipoles. The vdW, bond, angle, out-of-plane, and atomic polarizability parameters of ligands were transferred from the AMOEBA protein force field. The torsion parameters for the rotational bond were fitted to *ab initio* conformational energy profiles. The parametrization can be automated by using poltype program.⁸⁵

MD Simulation. All of the MD simulations in this study were performed using PMEMD and SANDER in AMBER⁹⁶ with the AMOEBA force field. TINKER⁸³ was used to prepare the initial systems. Two independent 5 ns MD simulations for the Zinc-finger protein were performed. The starting conformation was taken from the crystal structure (PDB entry: 1AAY⁸⁷) with DNA removed. The cysteine and histidine residues in the proximity of the Zn^{2+} ion were deprotonated on the Zn-bound N. On the basis of the crystal structure, HIS69, HIS84, HIS119, HIS123, and HIS129 are deprotonated at $N\epsilon$ while HIS97 is deprotonated at $N\delta$. The protein was placed in a periodic octahedral water box with at least 15 Å from the solute to the nearest box edge. Each simulation cell has 75 Å on each side, and it contains 9321 AMOEBA water molecules⁹⁹ and 11 Cl^- counterions, contributing to a total of 29 393 atoms. Two independent 5 ns MD simulations for the MMP protein complexes were also performed starting from the crystal structure (PDB entry: 1XUD⁸⁸). A similar periodic octahedral water box of 70 Å length on each side was set up with 23 470 atoms, including 6938 water molecules. The systems were minimized first and then heated up to 298 K gradually over 50 ps and then equilibrated for 225 ps under the NPT ensemble. The subsequent 5 ns MD simulations were performed in the NVT ensemble, with the density fixed at the NPT-average value and a time step of 1 fs. The temperature was maintained at 298 K using a Berendsen thermostat.⁸⁹ The vdW cutoff was set to 12 Å with long-tail correction applied. In all calculations, the long-range electrostatics were treated using Particle Mesh Ewald (PME) summation.^{90–92} The PME real space cutoff is set to 7 Å. The PME calculation used a $90 \times 90 \times 90$ grid and fifth-order B-spline interpolation. The induced dipoles were iterated until the root-mean-square change was below 0.01 D/

atom. Atomic coordinates of the simulation system were saved every 0.5 ps.

Binding Free Energy Calculation. The relative binding free energy of four pyrimidine dicarboxamide ligands (Figure 6) to MMP13 was calculated by alchemically transforming one ligand into another in both water and solvated protein complex. A scaling factor (λ) is used to divide the perturbation into intermediate steps. For example, ligand 1 ($\lambda = 0$) to ligand 2 ($\lambda = 1$) conversion can be expressed through 11 intermediate steps when $\lambda = \{0, 0.1, 0.2, 0.3, 0.4, 0.5, 0.6, 0.7, 0.8, 0.9, 1.0\}$. In both sets of simulations, the electrostatic interactions between ligand 1 and the surroundings were first perturbed to those of ligand 2 and the surroundings by scaling the electrostatic parameters of the two ligands linearly in 5–10 steps depending on the structural similarity of the ligands. Subsequently, the vdW interactions between the ligand and environment were transformed from ligand 1 to 2 in 5–10 steps, followed by valence terms (e.g., changing the equilibrium bond lengths from ligand 1 to 2) in 5–10 steps if applicable. During the decoupling of the vdW interactions, soft-core modifications⁹³ were introduced to the buffered 14–7 vdW potential function, to avoid the singularity problem at the end point:

$$U_{ij} = \lambda^n \epsilon_{ij} \frac{1.07^7}{[\alpha(1 - \lambda)^2 + (\rho + 0.07)^7]} \left(\frac{1.12}{\alpha(1 - \lambda)^2 + \rho^7 + 0.12} - 2 \right) \quad (2)$$

where the potential well depth ϵ_{ij} is in kcal/mol, ρ is the effective radius, and $\rho = R_{ij}/R_{ij}^0$. R_{ij} is the actual separation between i and j in Å, and R_{ij}^0 is the minimum energy distance. α is 0.07, and λ is the scaling factor.

MD simulations were performed at each step along the alchemical pathways for 2 ns for ligands in protein complexes and 1 ns for ligands in water. The Bennett Acceptance Ratio

Table 3. Heterodimer Binding Energies (kcal/mol) and Structures (Å) Computed by AMOEBA and *ab Initio* QM at Different Configurations (Shown in Figure 1)^a

configuration	<i>ab initio</i>		AMOEBA	
	distance	E_{int}	distance	E_{int}
conf. A: CH ₃ COO ⁻ -water (external)	1.65(O...H)	-17.39	1.74 (O...H)	-17.81
conf. B: CH ₃ COO ⁻ -water (bridge)	3.18 (C...O)	-20.99	3.18 (C...O)	-22.93
	1.96(O1...H1)		1.96(O1...H1)	
	1.96(O2...H2)		1.96(O2...H2)	
conf. C: CH ₃ COO ⁻ -Zn ²⁺ (external)	1.82(O...Zn)	-409.81 ^b	1.72(O...Zn)	-356.59
conf. D: CH ₃ COO ⁻ -Zn ²⁺ (bridge) ^c	2.25 (C...Zn)	-425.80 ^b	2.10 (C...Zn)	-442.30
	1.90(O...Zn)		1.81(O...Zn)	
conf. E: CH ₃ S ⁻ -water	2.14(S...H)	-16.36	2.14 (S...H)	-21.30
conf. F: CH ₃ S ⁻ -Zn ²⁺	2.24(S...Zn)	-421.78	2.06 (S...Zn)	-391.76
conf. G: imidazole-water	1.91 (N...H)	-8.20	2.11 (N...H)	-8.10
conf. H: imidazole-Zn ²⁺	1.85 (N...Zn)	-175.55	1.75 (N...Zn)	-172.25

^aThe *ab initio* results were obtained at the level of MP2/Aug-cc-pvtz with BSSE, unless otherwise noted. ^bAt the level of B3LYP6-311G**. ^cWith C-O-Zn angle at 150°.

estimator (BAR)⁹⁴ was used to compute the free energy differences between the adjacent intermediate steps:

$$\Delta A(j)_{\lambda_i \rightarrow \lambda_{i+1}} = -RT \ln \frac{\langle 1/[1 + \exp((E_{\lambda_i} - E_{\lambda_{i+1}} + C)/RT)] \rangle_{\lambda_{i+1}}}{\langle 1/[1 + \exp((E_{\lambda_{i+1}} - E_{\lambda_i} + C)/RT)] \rangle_{\lambda_i}} + C \quad (3)$$

where C is given by $C = \Delta A(j-1)_{\lambda_{i-1} \rightarrow \lambda_i}$ and j is the iteration index. Here, E_{λ_i} is the total energy of the system evaluated using

$$\Delta A(j)_{\lambda_i \rightarrow \lambda_{i+1}} = -RT \ln \frac{\langle [1 / (1 + \exp((E_{\lambda_i} - E_{\lambda_{i+1}} + C) / RT))] \times [\exp((E'_{\lambda_{i+1}} - E_{\lambda_{i+1}}) / RT)] \rangle_{\lambda_{i+1}}}{\langle \exp((E'_{\lambda_{i+1}} - E_{\lambda_{i+1}}) / RT) \rangle_{\lambda_{i+1}}} \frac{\langle [1 / (1 + \exp((E_{\lambda_{i+1}} - E_{\lambda_i} + C) / RT))] \times [\exp((E'_{\lambda_i} - E_{\lambda_i}) / RT)] \rangle_{\lambda_i}}{\langle \exp((E'_{\lambda_i} - E_{\lambda_i}) / RT) \rangle_{\lambda_i}} + C \quad (4)$$

where E'_{λ_i} is the total energy of the system evaluated at λ_i using a dipole convergence of 0.01 D, while E_{λ_i} indicates the potential energy evaluated using full convergence at 10⁻⁶ D per atom. λ' indicates the ensemble obtained using the looser dipole convergence. The reanalysis method was used, and the numerical reliability was verified. The comparison between using the BAR formula (eq 3) and using the reweighting BAR formula (eq 4) is discussed in Table 5.

RESULTS AND DISCUSSION

Dimers of Zn²⁺/Water Interacting with Model Compounds. We have first evaluated the Zn²⁺ or a water molecule interacting with each of the model compounds in both QM and AMOEBA calculations. The goal is to verify and systematically improve the AMOEBA parameters, especially atomic polarizability and vdW radii, of the three model compounds, the acetate anion, the methanthal anion, and imidazole. The first two ionic compounds were studied for the first time using AMOEBA. The purpose of examining both water and Zn²⁺ interacting with the same model compound is to avoid any biased changes in the model compound parameters. The AMOEBA atomic multipole parameters for three model compounds were obtained from QM calculations. The atomic polarizability values were mostly transferred from the AMOEBA parameter set, except for a few new types. For the

simulation snapshots at λ_j with a dipole convergence of 10⁻⁶ D. ΔA is solved iteratively until the value of $(\Delta A(j) - \Delta A(j-1))$ is less than 0.01 kcal/mol. While an induced dipole convergence (0.01 D per atom) has been used during the simulations for computational efficiency, a tighter convergence of 10⁻⁶ D per atom is applied to reanalyze the saved snapshots and compute the results. The reweighting is incorporated rigorously into the BAR formula:

oxygen atom in the acetate anion and the sulfur in CH₃S⁻, we found that atomic polarizability values larger than those in neutral molecules are necessary to reproduce the QM and experimental molecular polarizability (Tables 1 and 2). Previously, we also established that the atomic polarizabilities of the aromatic C and H in the benzene ring need to be greater than those of sp³ C and attached H atoms.⁶⁴ In order to reproduce the QM dimer energy and minimum-energy structure, increased polarizabilities are also needed for N and attached H in imidazole. Larger atomic polarizabilities in anions and aromatic molecules are expected given the excess electrons and more diffused electron clouds. The fact that larger vdW radii are needed for anionic atoms as compared to their neutral counterparts has been reported previously.^{32,33} Larger vdW radii (Table 2) than those in the neutral forms were also obtained by matching AMOEBA with the QM binding energy and geometry for both the Zn²⁺-model compound and water-model compound dimers. In Table 3, the final AMOEBA results are compared with *ab initio* values, and the binding energy differences and structure deviations are within 10% for all dimers except for CH₃S⁻-water and the bridge configuration of CH₃COO⁻-Zn²⁺. Note that the "constraint" here is that any change in the model compound vdW parameters will affect the Zn-model compound and water-model compound simultaneously. For example, decreasing the oxygen vdW radius

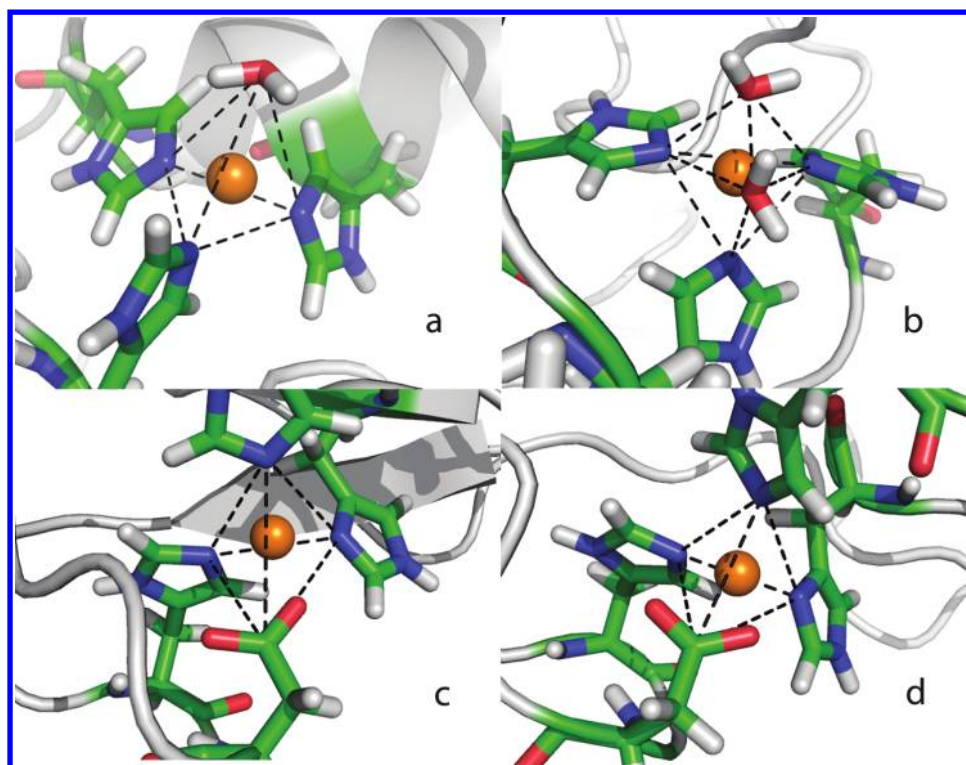


Figure 3. Structure comparison of the two zinc ions in the MMP13 complex (PDB entry: 1XUD): first zinc ion from the crystal structure in the tetrahedron (panel a), first zinc ion from the 5 ns MD simulation in trigonal bipyramidal geometry (panel b), second zinc ion from the crystal structure in bidentate tetrahedron (panel c), and second zinc ion from 5 ns MD simulation in bidentate tetrahedron (panel d).

in CH_3COO^- could lead to better agreement for the water– CH_3COO^- interaction but will also significantly overestimate the Zn^{2+} – CH_3COO^- attraction and pull them even closer than the QM distance. Similar trends were observed previously in fixed charge force fields.⁹⁵ The charge transfer effect accounts for this strongly anticooperative character in the polyligated complexes Zn^{2+} with anionic ligands,^{36,37} and it should also contribute, along with polarization effects, to the increase of the Zn–ligand distances optimized by quantum chemistry. In addition, it is observed that (Table 3) AMOEBA overestimated the energy gap between “bridge” (both oxygen atoms interacting with Zn in a bidentate fashion) and “external” (one oxygen forming a close interaction with Zn). The AMOEBA dimer energy for the “external” configuration is not as low as that of *ab initio*. It was noticed from the *ab initio* energy minimization of the “external” dimer that the C–O bond length involving the O that binds with Zn was 1.43 Å, the other C–O bond length was only 1.18 Å. The former is essentially a single bond, and the Zn^{2+} seems to have stabilized one of the “resonance” structures. Our force field has not been implemented to distinguish the two oxygens or the two C–O bonds in such cases.

MD Simulations of Zinc Proteins. We have investigated two zinc-binding proteins: (A) a zinc-finger system with three 4-fold coordinated zinc structural sites and (B) a MMP13 complex with one four-coordinated catalytic zinc binding site and another bidentate structural site. The results are presented in Figures 3–5 and are discussed below.

Zn^{2+} – Cys_2His_2 Motif from the Zn Finger Simulation. Starting from the X-ray structure of a zinc-finger protein (1AAY) containing three zinc ions, two independent 5 ns simulations have been performed. As we will show later, the change of coordination (due to subtle change in atom

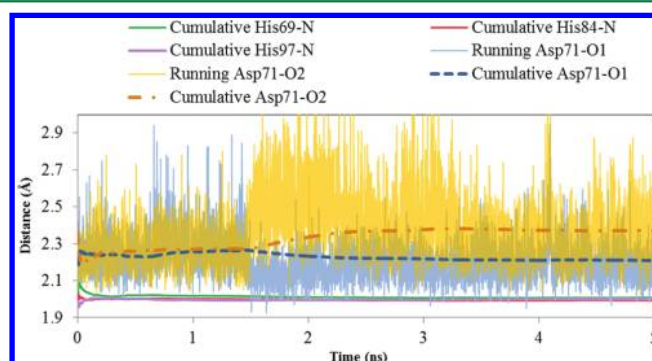


Figure 4. Interatomic distances between Zn^{2+} and its surrounding ligands during the 5 ns MD simulation.

polarizability) occurs within a few hundred picoseconds. All three zinc ions are coordinated with two histidines and two cysteines stably throughout the simulations. For all three Zn^{2+} binding sites, the root-mean-square deviations (RMSDs) of the backbone heavy atoms are 0.6, 0.6, and 0.8 Å from the X-ray structures. The average distances and angles are compared in Table 4. Overall, the zinc coordination structures given by AMOEBA are in very good agreement with the corresponding crystal structures. The average Zn–S distance obtained from simulation is 2.13 ± 0.05 Å, which is smaller than the distance of 2.25 ± 0.07 Å observed in the crystal structure. This slight difference is considered a consequence of optimizing the AMOEBA model against the *ab initio* calculation shown in Table 3. It is expected that implementing a charge transfer model into our AMOEBA polarizable potential can reproduce a more accurate Zn–S distance in both dimer interaction calculation and MD simulation.

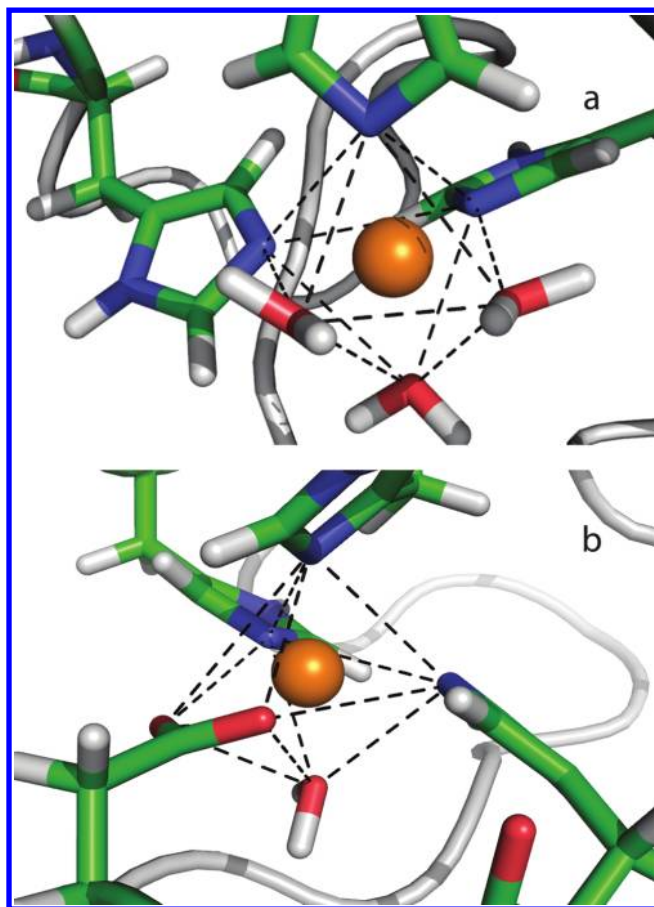


Figure 5. Under-polarization leads to 6-coordinated octahedral geometry for both His₃H₂O (panel a) and His₃Asp (panel b) Zn-binding sites in MMP-13. The corresponding crystal structures are shown in Figure 3.

Table 4. Comparison between MD and Experimental Averaged Zn Distances (Å) and Angles (degree) in the Zn-Finger Motif

		MD simulation	X-ray
Zn-finger	Zn-S	2.13(0.05)	2.25(0.07)
	Zn-N	2.10(0.07)	2.05(0.05)
	S-Zn-S	118.5(6.6)	115.8(1.1)
	N-Zn-N	93.9(5.2)	103.1(7.3)
	S-Zn-N	106.0(5.3)	110.3(4.5)
MMP	Zn-N	2.01(0.06)	2.13(0.03)
	Zn-O ₁	2.19(0.09)	2.01 ^a ; 1.92(0) ^b
	Zn-O ₂	2.41(0.18)	3.22 ^a ; 2.76(0.13) ^b

^aX-ray structure of protein complex 1XUD. ^bX-ray structures from Zn containing protein database survey.

Zn²⁺-His₃H₂O and Zn²⁺-His₃Asp Motif in MMP. We have also modeled a MMP13–ligand complex containing two zinc ions. Two independent 5 ns simulations starting from the X-ray crystal structure (1XUD) have been performed. For the first Zn²⁺ ion, there are three histidines and one water coordinating to form a tetrahedral structure, as shown in the crystal structure (Figure 3a). The three histidine residues were well maintained during the simulation, with an average Zn–N distance of 2.01 ± 0.06 Å. The water molecules were rather fluid and attempted to enter and leave the zinc coordination sphere during the 5 ns simulation. Water molecules and zinc were considered as

interacting with each other if the distance between them is less than 2.2 Å. Two water molecules were observed to interact with the zinc for approximately 75% of time, contributing to a 5-coordinated trigonal bipyramidal geometry (Figure 3b), with one of the water molecules occupying the fourth ligation site, as given in the crystal structure. For 25% of the simulation time, we observe the 4-coordinated tetrahedral geometry where only one water molecule was coordinating with Zn²⁺. Considering the fact that more than 30% of catalytic zinc proteins are 5-coordinated, as reported in the literature,¹³ this slight discrepancy seems to be reasonable and could be realistic dynamic behavior that is not captured by the X-ray structure. In addition, a previous QM/MM study of MMP2 based on B3LYP/OPLS-AA/PB also suggested that 5-coordination with three HIS residues and two waters is the most stable structure, although it was also pointed out that the energy differences among different coordinations are within the accuracy of DFT methods.⁹⁶

For the second zinc ion, three nitrogen atoms from the His residues plus two bidentate chelation of the Asp oxygen atoms form a bidentate tetrahedral coordination geometry (Figure 3c) in the crystal structure. Such a bidentate tetrahedral geometry was reproduced by our simulation, as shown in Figure 3d, and an alternation of the two oxygen atoms interacting with the zinc ion has been observed. During the 5 ns simulation, the average distance of Zn coordination for the closer oxygen was 2.21 ± 0.11 Å and that for the further one was 2.38 ± 0.17 Å, as shown in Figure 4; however, during the last 3.5 ns of simulation, the average distance became 2.19 ± 0.09 Å and 2.41 ± 0.18 Å, respectively. According to the analysis of the structural consensus of zinc coordination centers, the average distance of the zinc ion and the nearer and farther carboxylate oxygens is 1.92 ± 0 Å and 2.76 ± 0.13 Å in structural sites and 1.99 ± 0.06 Å and 2.58 ± 0.28 Å in catalytic sites, respectively.¹³ It is known that the conventional Coulomb scheme in the nonpolarizable force field has been deficient in describing bidentate chelation of Asp/Glu residues, and our AMOEBA model shows encouraging improvement. Nonetheless, as we discussed earlier, the inability of distinguishing the two oxygen atoms in COO⁻ by classical force fields results in an underestimation of binding energy of “external configuration” relative to the “bridge” one. Thus, the population of bidentate “bridge” configurations of Zn⋯COO⁻ was likely overestimated by the simulation. Additional contributions such as the charge transfer and perhaps charge flow are needed in the force fields in order to capture the bidentate vs external chelation more accurately.

Effect of Polarization on Zn²⁺ Coordination Geometry. We have demonstrated previously the importance of the polarization effect in treating zinc hydration.¹⁸ Here, we have also shown that with the induced dipole polarization, the AMOEBA model has yielded zinc coordination structures in very good agreement with the corresponding crystal structures. The Zn²⁺ parameters so far perform well in a range of different environments, from the water molecules to model compounds to protein complexes, without being “trained” on zinc enzyme complexes.

The importance of polarization effects is also revealed in this study: reduced atomic polarizabilities of the coordinating His residues would drive the coordination geometry to turn to octahedron in less than 1 ns. The coordination number of the zinc ion varies in different protein environments and with different enzyme functionalities; ion coordination numbers also play an important role in the different theories of selectivity.⁹⁷

A polarizable force field opens more of a possibility to describe variable zinc coordination reliably and address the different corresponding Zn enzyme functionalities. It has been reported that the picture of the ion coordination given by QM/MM simulations differs somewhat from the one provided by classical MD based on nonpolarizable force fields.⁹⁸ The inclusion of polarization effects seems critical.⁹⁹

To probe the effect of electronic polarization on the coordination geometry, we have performed two 2-ns simulations of the MMP-13 complex using a different set of atomic polarizability parameters for atoms on zinc-coordinating histidine rings. The atomic polarizability values were reduced (by ~20–30%) to those of nonaromatic elements as reported originally reported by Thole, i.e., 1.073 Å³ for C, 1.334 Å³ for N, and 0.496 Å³ for H. Interestingly, after ~1 ns MD simulations, the reduction in polarizability resulted in an octahedral structure for Zn²⁺ binding with (His)₃H₂O and (His)₃Asp (Figure 5), as witnessed in simulations using the fixed-charge force fields. Once the coordination turned to octahedron, it was unable to revert back in our simulations. Thus, underpolarization has yielded 6-coordinated Zn-binding sites, rather than the 4-coordination typically observed in experimental X-ray structures.

It has been reported that, for a nonpolarizable force field, a charge of +2 overestimates the coordination number of the zinc ions and “+1.5” is the most appropriate for MD simulations.²⁵ However, the stabilizing effect due to charge transfer cannot be captured through the “first order” Coulombic interaction of reduced charges. It should also be noted that appropriate vdW parameters for Zn²⁺ are also important for obtaining the correct coordination of the Zn–Cys₂His₂ binding site, as evidenced from earlier work by Sakharov and Lim.⁴³ In this work, we tried to separate the contribution by examining different physical properties. For example, the atomic polarizability was obtained by matching the *ab initio* molecular polarizability while the vdW parameters were refined using model compound dimer structures and energetics.

Binding Affinity Calculation for Pyrimidine Dicarboxamide Inhibitors Binding with MMP13. With reasonable success in modeling Zn binding with model compounds and proteins, we have further evaluated the free energy of inhibitors binding to Zn-containing MMP13. Although we are interested in inhibitors that directly chelate to the catalytic zinc ion with zinc binding groups (ZBGs), here we have chosen to study one of the earliest reported sets of nonzinc chelating inhibitors of MMP families. These four highly selective pyrimidine dicarboxamide inhibitors of MMP13 have binding free energies ranging from –7 to –11 kcal/mol, making an ideal system for evaluating our zinc model in free energy calculations (Figure 6). Generally, the nonzinc chelating inhibitors can overcome the nonselective toxicity. The zinc ion does not “directly” interact with these inhibitors, but the shortest distances between the Zn ion and the inhibitor heavy atoms is only 4.7 Å. To compute the relative binding free energy among the four ligands, ligands 2 through 3 were alchemically transformed from ligand 4, and ligand 2 was transformed into ligand 1. The experimental binding free energies are based on inhibition constants determined by isothermal titration calorimetry under various assay conditions.¹⁰⁰

The calculated relative binding free energies are in agreement with experimental measurements (Table 5) with a RMSD of 0.72 kcal/mol. The calculated relative binding free energies have been offset by the experimental binding free energy of

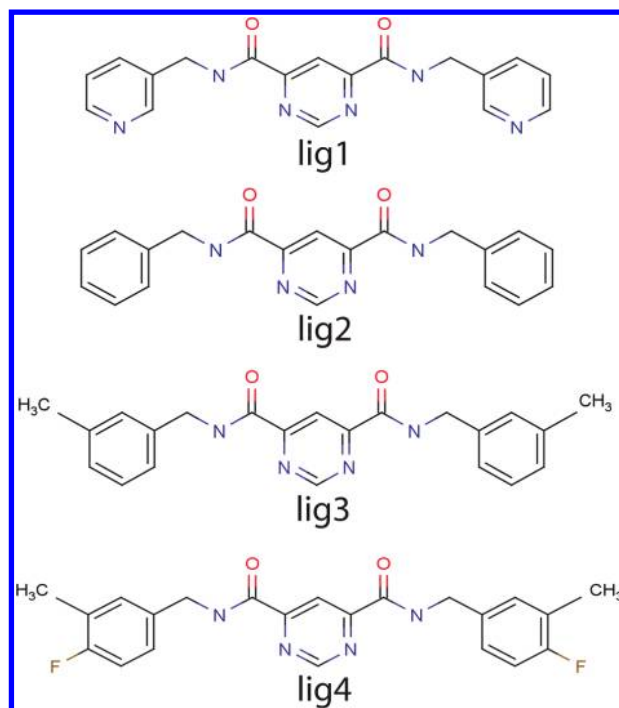


Figure 6. Pyrimidine dicarboxamide inhibitors binding with MMP-13.

MMP13–ligand 4 and plotted in Figure 7. A correlation coefficient (*R*) of 0.95 between the calculated and experimental binding free energy was obtained.¹⁰⁰ Using BAR and BAR reweighting procedures gave us similar merits.

Despite the limited data points, we observe a noticeable correlation between binding free energy and polarizability, i.e., the stronger the molecular polarizability, the more favorable the binding affinity is. For ligands 1, 2, 3, and 4, the molecular polarizability values are 28.4, 29.5, 32.3, and 32.4 Å³, respectively, and the experimental binding affinities are –7.07, –8.73, –9.75, and –11.05 kcal/mol. We have previously reported a similar trend for the trypsin–benzamide ligands.¹⁰¹

To probe the role of the zinc electrostatics on the binding, we performed a virtual experiment where the zinc ion charge was switched off from +2 to 0. The relative binding free energies among the four inhibitors were re-evaluated by using the same MD trajectories obtained from Zn²⁺ simulations. Removing the Zn²⁺ +2 charge led to a significant and consistent overestimation of relative binding free energy differences (Figure 7). The RMSD between experimental and calculated relative binding affinity became ~2.2 kcal/mol. It suggests that the effect of zinc charge does not “cancel” between the different inhibitors binding to MMP13. Instead, the presence of Zn²⁺ seems to minimize the affinity gaps among the tested inhibitors.

We also performed an additional test where the polarization due to the zinc ion is turned off in the system but the +2 charge on zinc was kept. The relative binding free energies were again re-evaluated using the same MD trajectories (Table 5). Compared to the “BAR” scheme with full parameters, setting the Zn charge to 0 generated less favorable relative binding free energies, and turning off Zn polarization seemed to generate more favorable relative binding free energies, which is consistent with the findings of our previous study of trypsin–benzamide binding.⁶⁶ More interestingly, neglecting the polarization effect of the zinc ion led to a deviated ranking

Table 5. Relative Binding Free Energies from Alchemical Perturbation Calculations (kcal/mol)^a

	BAR (eq 3)			reweighting BAR (eq 4)			BAR with Zn charge set to 0			BAR without polarization by Zn ²⁺			experiment results
	$\Delta G_{\text{lig-wat}}$	$\Delta G_{\text{lig-pro}}$	$\Delta\Delta G$	$\Delta G_{\text{lig-wat}}$	$\Delta G_{\text{lig-pro}}$	$\Delta\Delta G$	$\Delta G_{\text{lig-wat}}$	$\Delta G_{\text{lig-pro}}$	$\Delta\Delta G$	$\Delta G_{\text{lig-wat}}$	$\Delta G_{\text{lig-pro}}$	$\Delta\Delta G$	$\Delta\Delta G_{\text{expt}}^b$
4→3	4.14	5.52	1.38	4.14	5.55	1.41	4.14	5.82	1.68	4.14	5.29	1.15	1.30
4→2	11.94	13.45	1.51	13.47	15.15	1.68	11.94	15.01	3.07	11.94	13.02	1.08	2.32
2→1	-10.07	-9.36	0.71	-9.77	-9.30	0.46	-10.07	-5.52	4.55	-10.07	-10.85	-0.62	1.66

^aIn the BAR procedure, the simulation was performed using an induced-dipole convergence of 0.01 D per atom, and the free energy was evaluated with a tighter convergence (10^{-6}) using eq 3. The reweighting BAR introduces a rigorous reweighting due to the different polarization convergence based on eq 4. ^bRef 100.

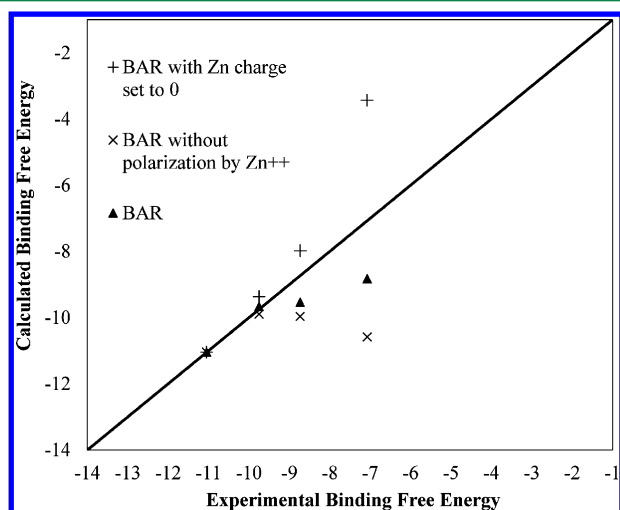


Figure 7. Comparison of calculated and experimental relative binding free energies (kcal/mol). Ligands 4, 3, 2, and 1 can be identified from the *x* axis in order from left to right, respectively, with the corresponding experimental binding free energies -11.05 , -9.75 , -8.73 , and -7.07 kcal/mol.

order. This suggests that the polarization effect due to the zinc ion is not systematic but inhibitor-dependent. This would make it difficult for nonpolarizable force fields to capture the polarization effect implicitly, e.g., by scaling the ligand charges. The decisive role of polarization in enabling a correct ranking of competing inhibitors to a given protein target has also been demonstrated recently, such as in the complexes of pyrrolopyrimidine inhibitors to the FAK kinase¹⁰² and mannose phosphate/malonate surrogates to the phosphomannoisomerase Zn-metalloenzyme.¹⁰³

CONCLUSION

Metal ions play indispensable roles in protein structure and function, as nearly one-third of all proteins contain metal ions. Understanding the Zn–protein binding, in particular, the factors governing specificity and coordination geometry, is crucial for the development of novel ligands for existing Zn binding sites as well as the *de novo* design of new Zn-binding proteins.

Polarizable force fields hold the promise for treating metal ions in proteins in an effective way, by explicitly taking into account the polarization and potentially the charge-transfer effects. In the AMOEBA polarizable potential, the polarization effect is treated via atomic dipole induction. In a previous study, we have shown that charge transfer effect in Zn²⁺ binding clusters diminishes moving from the gas-phase toward the condensed-phase and to some extent can be incorporated into the dipole polarization.¹⁸ In this study, we have examined Zn²⁺

interacting with common ligands in a protein environment. We have refined the atomic polarizability and vdW parameters of a few atom types in the His, charged Cys, and Asp residue side chains by assessing their interactions with Zn²⁺ and the water molecule, respectively. Extensive MD simulations of two zinc-containing enzyme systems with different coordinating ligands, including a bidentate tetrahedral binding site, has yielded reasonable zinc coordination geometry and binding distances in comparison with the X-ray crystal structures. More interestingly, we found that the coordination geometry is very sensitive to the polarizabilities of the coordinating ligands. Under-polarization leads to 6-coordination instead of the 4-coordination that is typically observed experimentally.

The relative binding free energies of four MMP13 inhibitors have been calculated to be in good agreement with experimental measurements. While there is a moderate separation distance between the zinc ion and the inhibitors, the +2 net charge on zinc has a strong influence on the inhibitor relative binding affinities. The polarizing field from the zinc ion also contributes to the binding energetics but in an inhibitor-dependent way, as expected from the many-bodied nature of the polarization effect. The AMOEBA polarizable force field has demonstrated its capacity for accurate description of Zn–protein interactions. The results obtained in this study encourage a broader investigation of ligand binding to metalloproteins using polarizable force fields, including those directly involving metal ions at the binding site. Meanwhile, efforts to include the short-range charge transfer and penetration functionalities into the AMOEBA polarizable multipole model is ongoing, which is expected to further improve our ability to model complex ion–protein interactions.

ASSOCIATED CONTENT

Supporting Information

The comparative tables comparing *ab initio* and AMOEBA. This information is available free of charge via the Internet at <http://pubs.acs.org>.

AUTHOR INFORMATION

Corresponding Author

*E-mail: pren@mail.utexas.edu.

Notes

The authors declare no competing financial interest.

ACKNOWLEDGMENTS

We thank the National Institute of General Medical Sciences (R01GM079686) and Robert A. Welch foundation (F-1691) for support. The HPC resources were provided by the National Science Foundation through TeraGrid and the Texas Advanced Computing Center (TACC) under grant number TG-

MCB100057. W.Y. is grateful for the funding support (MCB 0919983) by National Science Foundation.

REFERENCES

- (1) Tainer, J. A.; Roberts, V. A.; Getzoff, E. D. *Curr. Opin. Biotechnol.* **1991**, *2*, 582–591.
- (2) Wriggers, W.; Mehler, E.; Pitici, F.; Weinstein, H.; Schulten, K. *Biophys. J.* **1998**, *74*, 1622–1639.
- (3) Xiao, B.; Heath, R.; Saiu, P.; Leiper, F. C.; Leone, P.; Jing, C.; Walker, P. A.; Haire, L.; Eccleston, J. F.; Davis, C. T.; Martin, S. R.; Carling, D.; Gamblin, S. J. *Nature* **2007**, *449*, 496–U414.
- (4) Lee, S. B.; Warthaka, M.; Yan, C. L.; Kaoud, T. S.; Piserchio, A.; Ghose, R.; Ren, P. Y.; Dalby, K. N. *PLoS One* **2011**, *6*.
- (5) Ivano Bertini, A. S.; Sigel, H. *Handbook on metalloproteins* **2001**.
- (6) Christianson, D. W. *Adv. Protein Chem.* **1991**, *42*, 281–355.
- (7) Parkin, G. *Chem. Rev.* **2004**, *104*, 699–767.
- (8) Lipscomb, W. N.; Strater, N. *Chem. Rev.* **1996**, *96*, 2375–2433.
- (9) Wilcox, D. E. *Chem. Rev.* **1996**, *96*, 2435–2458.
- (10) Murakami, M.; Hirano, T. *Cancer Sci.* **2008**, *99*, 1515–1522.
- (11) Chaturvedi, U. C.; Shrivastava, R. *FEMS Immunol. Med. Microbiol.* **2005**, *43*, 105–114.
- (12) Lee, Y. M.; Lim, C. J. *Mol. Biol.* **2008**, *379*, 545–553.
- (13) Patel, K.; Kumar, A.; Durani, S. *Biochim. Biophys. Acta, Proteins Proteomics* **2007**, *1774*, 1247–1253.
- (14) Vallee, B. L.; Falchuk, K. H. *Physiol. Rev.* **1993**, *73*, 79–118.
- (15) Raha, K.; Merz, K. M. *J. Am. Chem. Soc.* **2004**, *126*, 1020–1021.
- (16) Fatmi, M. Q.; Hofer, T. S.; Rode, B. M. *Phys. Chem. Chem. Phys.* **2010**, *12*, 9713–9718.
- (17) Fatmi, M. Q.; Hofer, T. S.; Randolf, B. R.; Rode, B. M. *J. Phys. Chem. B* **2007**, *111*, 151–158.
- (18) Wu, J. C.; Piquemal, J. P.; Chaudret, R.; Reinhardt, P.; Ren, P. Y. *J. Chem. Theory Comput.* **2010**, *6*, 2059–2070.
- (19) Wang, C.; Vernon, R.; Lange, O.; Tyka, M.; Baker, D. *Protein Sci.* **2010**, *19*, 494–506.
- (20) Donini, O. A. T.; Kollman, P. A. *J. Med. Chem.* **2000**, *43*, 4180–4188.
- (21) Merz, K. M.; Kollman, P. A. *J. Am. Chem. Soc.* **1989**, *111*, 5649–5658.
- (22) Demoulin, D.; Pullman, A. *Theor. Chim. Acta* **1978**, *49*, 161–181.
- (23) Kothekar, V.; Pullman, A.; Demoulin, D. *Int. J. Quantum Chem.* **1978**, *14*, 779–791.
- (24) Stote, R. H.; Karplus, M. *Proteins: Struct., Funct., Genet.* **1995**, *23*, 12–31.
- (25) Koca, J.; Zhan, C. G.; Rittenhouse, R. C.; Ornstein, R. L. *J. Comput. Chem.* **2003**, *24*, 368–378.
- (26) Hoops, S. C.; Anderson, K. W.; Merz, K. M. *J. Am. Chem. Soc.* **1991**, *113*, 8262–8270.
- (27) Toba, S.; Damodaran, K. V.; Merz, K. M. *J. Med. Chem.* **1999**, *42*, 1225–1234.
- (28) Zhang, W.; Hou, T. J.; Qiao, X. B.; Huai, S.; Xu, X. J. *J. Mol. Model.* **2004**, *10*, 112–120.
- (29) Roe, R. R.; Pang, Y. P. *J. Mol. Model.* **1999**, *5*, 134–140.
- (30) Calimet, N.; Simonson, T. *J. Mol. Graphics Modell.* **2006**, *24*, 404–411.
- (31) Gresh, N.; Derreumaux, P. *J. Phys. Chem. B* **2003**, *107*, 4862–4870.
- (32) Gresh, N.; Piquemal, J. P.; Krauss, M. *J. Comput. Chem.* **2005**, *26*, 1113–1130.
- (33) Gresh, N. *J. Comput. Chem.* **1995**, *16*, 856–882.
- (34) Garmer, D. R.; Gresh, N.; Roques, B. P. *Proteins: Struct., Funct., Bioinf.* **1998**, *31*, 42–60.
- (35) Gresh, N.; Roques, B. P. *Biopolymers* **1997**, *41*, 145–164.
- (36) Tiraboschi, G.; Gresh, N.; Giessner-Prettre, C.; Pedersen, L. G.; Deerfield, D. W. *J. Comput. Chem.* **2000**, *21*, 1011–1039.
- (37) Tiraboschi, G.; Roques, B. P.; Gresh, N. *J. Comput. Chem.* **1999**, *20*, 1379–1390.
- (38) Antony, J.; Gresh, N.; Olsen, L.; Hemmingsen, L.; Schofield, C. J.; Bauer, R. *J. Comput. Chem.* **2002**, *23*, 1281–1296.
- (39) Antony, J.; Piquemal, J. P.; Gresh, N. *J. Comput. Chem.* **2005**, *26*, 1131–1147.
- (40) Jenkins, L. M. M.; Hara, T.; Durell, S. R.; Hayashi, R.; Inman, J. K.; Piquemal, J. P.; Gresh, N.; Appella, E. *J. Am. Chem. Soc.* **2007**, *129*, 11067–11078.
- (41) Roux, C.; Gresh, N.; Perera, L. E.; Piquemal, J. P.; Salmon, L. *J. Comput. Chem.* **2007**, *28*, 938–957.
- (42) Roux, C.; Bhatt, F.; Foret, J.; de Courcy, B.; Gresh, N.; Piquemal, J. P.; Jeffery, C. J.; Salmon, L. *Proteins: Struct., Funct., Bioinf.* **2011**, *79*, 203–220.
- (43) Sakharov, D. V.; Lim, C. *J. Am. Chem. Soc.* **2005**, *127*, 4921–4929.
- (44) Urnov, F. D.; Miller, J. C.; Lee, Y. L.; Beausejour, C. M.; Rock, J. M.; Augustus, S.; Jamieson, A. C.; Porteus, M. H.; Gregory, P. D.; Holmes, M. C. *Nature* **2005**, *435*, 646–651.
- (45) Li, W. F.; Zhang, J.; Wang, J.; Wang, W. *J. Am. Chem. Soc.* **2008**, *130*, 892–900.
- (46) Winum, J. Y.; Scozzafava, A.; Montero, J. L.; Supuran, C. T. *Curr. Pharm. Des.* **2008**, *14*, 615–621.
- (47) Hu, J. L.; Van den Steen, P. E.; Sang, Q. X. A.; Opdenakker, G. *Nat. Rev. Drug Discovery* **2007**, *6*, 480–498.
- (48) Durrant, J. D.; de Oliveira, C. A. F.; McCammon, J. A. *J. Mol. Recognit.* **2010**, *23*, 173–182.
- (49) Dejonckheere, E.; Libert, C.; Vandenbroucke, R. *Drug Discovery Today* **2011**, *16*, 762–778.
- (50) Sang, Q. X. A.; Jin, Y. H.; Newcomer, R. G.; Monroe, S. C.; Fang, X. X.; Hurst, D. R.; Lee, S.; Cao, Q.; Schwartz, M. T. *A. Curr. Top. Med. Chem.* **2006**, *6*, 289–316.
- (51) Durrant, J. D.; de Oliveira, C. A. F.; McCammon, J. A. *Chem. Biol. Drug Des.* **2011**, *78*, 191–198.
- (52) Cuniase, P.; Devel, L.; Makaritis, A.; Beau, F.; Georgiadis, D.; Matziari, A.; Yiotakis, A.; Dive, V. *Biochimie* **2005**, *87*, 393–402.
- (53) Jacobsen, E. J.; Mitchell, M. A.; Hendges, S. K.; Belonga, K. L.; Skaletzky, L. L.; Stelzer, L. S.; Lindberg, T. J.; Fritzen, E. L.; Schostarez, H. J.; O'Sullivan, T. J.; Maggiora, L. L.; Stuchly, C. W.; Laborde, A. L.; Kubicek, M. F.; Poorman, R. A.; Beck, J. M.; Miller, H. R.; Petzold, G. L.; Scott, P. S.; Truesdell, S. E.; Wallace, T. L.; Wilks, J. W.; Fisher, C.; Goodman, L. V.; Kaytes, P. S.; Ledbetter, S. R.; Powers, E. A.; Vogeli, G.; Mott, J. E.; Trepod, C. M.; Staples, D. J.; Baldwin, E. T.; Finzel, B. C. *J. Med. Chem.* **1999**, *42*, 1525–1536.
- (54) Dublanchet, A. C.; Ducrot, P.; Andrianjara, C.; O'Gara, M.; Morales, R.; Compere, D.; Denis, A.; Blais, S.; Cluzeau, P.; Courte, K.; Hamon, J.; Moreau, F.; Prunet, M. L.; Tertre, A. *Bioorg. Med. Chem. Lett.* **2005**, *15*, 3787–3790.
- (55) Pochetti, G.; Montanari, R.; Gege, C.; Chevrier, C.; Taveras, A. G.; Mazza, F. *J. Med. Chem.* **2009**, *52*, 1040–1049.
- (56) Ren, P. Y.; Ponder, J. W. *J. Comput. Chem.* **2002**, *23*, 1497–1506.
- (57) Halgren, T. A. *J. Am. Chem. Soc.* **1992**, *114*, 7827–7843.
- (58) Ponder, J. W.; Wu, C. J.; Ren, P. Y.; Pande, V. S.; Chodera, J. D.; Schnieders, M. J.; Haque, I.; Mobley, D. L.; Lambrecht, D. S.; DiStasio, R. A.; Head-Gordon, M.; Clark, G. N. I.; Johnson, M. E.; Head-Gordon, T. *J. Phys. Chem. B* **2010**, *114*, 2549–2564.
- (59) Ren, P. Y.; Ponder, J. W. *J. Phys. Chem. B* **2003**, *107*, 5933–5947.
- (60) Ren, P. Y.; Ponder, J. W. *J. Phys. Chem. B* **2004**, *108*, 13427–13437.
- (61) Grossfield, A.; Ren, P. Y.; Ponder, J. W. *J. Am. Chem. Soc.* **2003**, *125*, 15671–15682.
- (62) Jiao, D.; King, C.; Grossfield, A.; Darden, T. A.; Ren, P. Y. *J. Phys. Chem. B* **2006**, *110*, 18553–18559.
- (63) Piquemal, J. P.; Perera, L.; Cisneros, G. A.; Ren, P. Y.; Pedersen, L. G.; Darden, T. A. *J. Chem. Phys.* **2006**, *125*.
- (64) Ren, P. Y.; Wu, C. J.; Ponder, J. W. *J. Chem. Theory Comput.* **2011**, *7*, 3143–3161.
- (65) Shi, Y.; Wu, C. J.; Ponder, J. W.; Ren, P. Y. *J. Comput. Chem.* **2011**, *32*, 967–977.
- (66) Jiao, D.; Golubkov, P. A.; Darden, T. A.; Ren, P. *Proc. Natl. Acad. Sci. U. S. A.* **2008**, *105*, 6290–6295.

- (67) Jiao, D.; Zhang, J. J.; Duke, R. E.; Li, G. H.; Schnieders, M. J.; Ren, P. Y. *J. Comput. Chem.* **2009**, *30*, 1701–1711.
- (68) Schnieders, M. J.; Fenn, T. D.; Pande, V. S. *J. Chem. Theory Comput.* **2011**, *7*, 1141–1156.
- (69) Fenn, T. D.; Schnieders, M. J.; Brunger, A. T.; Pande, V. S. *Biophys. J.* **2010**, *98*, 2984–2992.
- (70) Schnieders, M. J.; Fenn, T. D.; Pande, V. S.; Brunger, A. T. *Acta Crystallogr., Sect. D: Biol. Crystallogr.* **2009**, *65*, 952–965.
- (71) Clavaguera, C.; Dognon, J. P.; Pyykko, P. *Chem. Phys. Lett.* **2006**, *429*, 8–12.
- (72) Clavaguera, C.; Pollet, R.; Soudan, J. M.; Brenner, V.; Dognon, J. P. *J. Phys. Chem. B* **2005**, *109*, 7614–7616.
- (73) Clavaguera, C.; Sansot, E.; Calvo, F.; Dognon, J. P. *J. Phys. Chem. B* **2006**, *110*, 12848–12851.
- (74) Rogers, D. M.; Beck, T. L. *J. Chem. Phys.* **2010**, 132.
- (75) Tuma, L.; Jenicek, D.; Jungwirth, P. *Chem. Phys. Lett.* **2005**, *411*, 70–74.
- (76) Zhao, Z.; Rogers, D. M.; Beck, T. L. *J. Chem. Phys.* **2010**, 132.
- (77) Jiang, J. L.; Wu, Y. B.; Wang, Z. X.; Wu, C. J. *Chem. Theory Comput.* **2010**, *6*, 1199–1209.
- (78) Kaminsky, J.; Jensen, F. J. *Chem. Theory Comput.* **2007**, *3*, 1774–1788.
- (79) Liang, T.; Walsh, T. R. *Phys. Chem. Chem. Phys.* **2006**, *8*, 4410–4419.
- (80) Liang, T.; Walsh, T. R. *Mol. Simul.* **2007**, *33*, 337–342.
- (81) Burnham, C. J.; Li, J. C.; Xantheas, S. S.; Leslie, M. J. *Chem. Phys.* **1999**, *110*, 4566–4581.
- (82) Stone, A. J. GDMA. <http://www-stone.ch.cam.ac.uk/documentation/gdma/> (accessed: May 2001, 2011).
- (83) Ponder, J. W. Tinker Molecular Modeling. <http://dasher.wustl.edu/tinker/> (accessed: July 2, 2010).
- (84) Frisch, M. J.; Trucks, G. W.; Schlegel, H. B.; Scuseria, G. E.; Robb, M. A.; Cheeseman, J. R.; Montgomery, J. A., Jr.; Vreven, T.; Kudin, K. N.; Burant, J. C.; Millam, J. M.; Iyengar, S. S.; Tomasi, J.; Barone, V.; Mennucci, B.; Cossi, M.; Scalmani, G.; Rega, N.; Petersson, G. A.; Nakatsuji, H.; Hada, M.; Ehara, M.; Toyota, K.; Fukuda, R.; Hasegawa, J.; Ishida, M.; Nakajima, T.; Honda, Y.; Kitao, O.; Nakai, H.; Klene, M.; Li, X.; Knox, J. E.; Hratchian, H. P.; Cross, J. B.; Bakken, V.; Adamo, C.; Jaramillo, J.; Gomperts, R.; Stratmann, R. E.; Yazyev, O.; Austin, A. J.; Cammi, R.; Pomelli, C.; Ochterski, J. W.; Ayala, P. Y.; Morokuma, K.; Voth, G. A.; Salvador, P.; Dannenberg, J. J.; Zakrzewski, V. G.; Dapprich, S.; Daniels, A. D.; Strain, M. C.; Farkas, O.; Malick, D. K.; Rabuck, A. D.; Raghavachari, K.; Foresman, J. B.; Ortiz, J. V.; Cui, Q.; Baboul, A. G.; Clifford, S.; Cioslowski, J.; Stefanov, B. B.; Liu, G.; Liashenko, A.; Piskorz, P.; Komaromi, I.; Martin, R. L.; Fox, D. J.; Keith, T.; Al-Laham, M. A.; Peng, C. Y.; Nanayakkara, A.; Challacombe, M.; Gill, P. M. W.; Johnson, B.; Chen, W.; Wong, M. W.; Gonzalez, C.; Pople, J. A. *Gaussian 03*; Gaussian, Inc.: Pittsburgh, PA, 2003.
- (85) Wu, J. C.; Chatterjee, G.; Ren, P. Y. *Theor. Chem. Acc.* **2011**.
- (86) Case, D. A.; Cheatham, T. E.; Darden, T.; Gohlke, H.; Luo, R.; Merz, K. M.; Onufriev, A.; Simmerling, C.; Wang, B.; Woods, R. J. *J. Comput. Chem.* **2005**, *26*, 1668–1688.
- (87) ElrodErickson, M.; Rould, M. A.; Nekludova, L.; Pabo, C. O. *Structure* **1996**, *4*, 1171–1180.
- (88) Wasserman, Z. R. *Chem. Biol.* **2005**, *12*, 143–144.
- (89) Berendsen, H. J. C.; Postma, J. P. M.; Vangunsteren, W. F.; Dinola, A.; Haak, J. R. *J. Chem. Phys.* **1984**, *81*, 3684–3690.
- (90) Essmann, U.; Perera, L.; Berkowitz, M. L.; Darden, T.; Lee, H.; Pedersen, L. G. *J. Chem. Phys.* **1995**, *103*, 8577–8593.
- (91) Darden, T.; York, D.; Pedersen, L. *J. Chem. Phys.* **1993**, *98*, 10089–10092.
- (92) Sagui, C.; Darden, T. A. *Annu. Rev. Biophys. Biomol. Struct.* **1999**, *28*, 155–179.
- (93) Beutler, T. C.; Mark, A. E.; Vanschaik, R. C.; Gerber, P. R.; van Gunsteren, W. F. *Chem. Phys. Lett.* **1994**, *222*, 529–539.
- (94) Bennett, C. H. *J. Comput. Phys.* **1976**, *22*, 245–268.
- (95) Brandt, E. G.; Hellgren, M.; Brinck, T.; Bergman, T.; Edholm, O. *Phys. Chem. Chem. Phys.* **2009**, *11*, 975–983.
- (96) Diaz, N.; Suarez, D.; Sordo, T. L. *J. Phys. Chem. B* **2006**, *110*, 24222–24230.
- (97) Varma, S.; Rempe, S. B. *Biophys. J.* **2007**, *93*, 1093–1099.
- (98) Bucher, D.; Guidoni, L.; Carloni, P.; Rothlisberger, U. *Biophys. J.* **2010**, *98*, L47–L49.
- (99) Bucher, D.; Rothlisberger, U. *J. Gen. Physiol.* **2010**, *135*, 549–554.
- (100) Engel, C. K.; Pirard, B.; Schimanski, S.; Kirsch, R.; Habermann, J.; Klingler, O.; Schlotte, V.; Weithmann, K. U.; Wendt, K. U. *Chem. Biol.* **2005**, *12*, 181–189.
- (101) Shi, Y.; Jiao, D. A.; Schnieders, M. J.; Ren, P. Y. *Annu. Int. Conf. IEEE Eng. Med. Biol. Soc.* **2009**, *1*, 2328–2331.
- (102) de Courcy, B.; Piquemal, J. P.; Garbay, C.; Gresh, N. *J. Am. Chem. Soc.* **2010**, *132*, 3312–3320.
- (103) Gresh, N.; de Courcy, B.; Piquemal, J. P.; Foret, J.; Courtiol-Legourd, S.; Salmon, L. *J. Phys. Chem. B* **2011**, *115*, 8304–8316.
- (104) Voisin, C.; Cartier, A.; Rivail, J. L. *J. Phys. Chem.* **1992**, *96*, 7966–7971.
- (105) Zope, R. R.; Baruah, T.; Pederson, M. R.; Dunlap, B. I. *Int. J. Quantum Chem.* **2008**, *108*, 307–317.
- (106) Calderbank, K. E.; Calvert, R. L.; Lukins, P. B.; Ritchie, G. L. D. *Aust. J. Chem.* **1981**, *34*, 1835–1844.
- (107) Carles, S.; Lecomte, F.; Schermann, J. P.; Desfrancois, C. *J. Phys. Chem. A* **2000**, *104*, 10662–10668.